A simplified ω-ALDF rank-correlated full-spectrum k-distribution model for combustion applications

Jean-Louis Consalvi, Fatiha Nmira, Frédéric André, Vladimir Solovjov, Brent Webb

A simplified ω-ALDF rank-correlated full-spectrum k-distribution model for combustion applications

Jean-Louis Consalvi[1,*], Fatiha Nmira[2], Frédéric André[3], Vladimir P. Solovjov[4], Brent W. Webb[4]

1 Aix-Marseille Université, IUSTI UMR 7343, 5 rue E. Fermi, 13453 Marseille cedex 13, France

2 Direction R&D EDF, 6 Quai Watier, 78401 Chatou Cedex, France

3 Univ Lyon, CNRS, INSA-Lyon, CETHIL UMR5008, F-69621 Villeurbanne, France

4 Brigham Young University, 360G EB, Provo, UT 84602, USA

* Corresponding author: jean-louis.consalvi@univ-amu.fr

Abstract.

The objective of this paper is to present a method that allows simplifying the use of ω-absorption line distribution functions (ω-ALDF) inside rank correlated full-spectrum k-distribution (RCFSK) models for application in combustion problems. In this simplified version, the ω-ALDF is constructed without any *a priori* information on the problem treated. It can be used directly but, in order to simplify further the concept for possible users, we suggest here approximating this ω-ALDF using an Absorption Line Blackbody Distribution Function (ALBDF) at a temperature defined in terms of the ω-ALDF. The method is validated in some combustion scenarios. The model is assessed by comparison with a narrow band correlated-k (NBCK) model through decoupled radiative simulations of eight turbulent axisymmetric non-premixed jet flames covering a wide range of optical-thicknesses and contributions of soot to radiation. The predictions are within 4% of the reference solution. A consequence of the proposed approach is that the FSCK parameters, namely the absorption coefficient and the stretching function, depends only on local variables. This allows one to forgo the specification

of an arbitrary blackbody source temperature, and to develop a specific storage strategy to provide an efficient model for Computational Fluid Dynamics (CFD) simulations of combustion problems.

Key words: gas radiative property model, ω-ALDF, RCFSK, combustion applications

1. Introduction

The development of high-fidelity computational fluid dynamics models for combustion applications has naturally raised the choice of relevant gas radiative property models requiring a compromise between accuracy and computational efficiency [1]. For this purpose, global models based on the *k*-distribution concept, namely the Spectral Line Weighted-sum-of-gray-gases (SLW) [2] and the Full-Spectrum Correlated-*k* (FSCK) [3] methods, have been extensively developed and tested over the last twenty years and have emerged as the best candidates for coupled high-fidelity simulations of combustion problems. They were proved to be accurate and can be applied to arbitrary mixtures of gases and non-gray absorbing gray-scattering particles [1],[4],[5]. In addition, the development of look-up tables has significantly improved their computational efficiency [6] - [8] while the subsequent development of machine learning-fitted look-up table reduced considerably the required memory size [9], [10]. Among the different schemes, those proposed by Cai and Modest [11] and the Rank Correlated (RC) FSK/SLW model [12], [13] preserve emission and were found to be overall the most accurate and the most robust [14], [15]. In addition, it was found that the RC methods do not require specification of a reference gas thermodynamic state and are only weakly sensitive to the Planck blackbody temperature [12]-[14]. André et al. developed a universal RCFSK/SLW model, the ω-ALDF based RCFSK/RCSLW model, that also eliminates the need for the specification of the Planck blackbody temperature [16]. As a reasonable approximation, the RCFSK method was applied to large eddy simulations of non-sooting and sooting pool fires by fixing the

Planck-temperature to an arbitrary constant value of 1500 K [17]-[20]. This approach was found to yield an efficient implementation of the RCSFK models as the model parameters, namely the absorption coefficient and the stretching functions, then depend only on local scalars, such as species mole fractions, soot volume fraction, and temperature. They can be stored in a "flamelet" library as a function of a reduced set of manifolds. As a consequence, the computational effort during the simulations to determine these parameters is small, only requiring simple multi-dimensional interpolations.

The objective of this study is twofold: i) to justify theoretically the choice of a constant value for the Planck blackbody temperature when building a RCFSK/RCSLW model database for combustion applications, and ii) to assess the predictive accuracy of this simplified ω-ALDF based RCFSK method through a series of simulations involving turbulent jet flames over a wide range of optical thicknesses and soot contributions to radiation.

This work is organized as follows. Section 2 presents the gas radiative property models while Section 3 describe the test cases and the metrics. Section 4 is devoted to the results and discussions, and finally, Section 5 summarizes the conclusions.

2. Gas radiative property models

The radiating species are H_2O, CO_2 and soot and the covered spectral interval is 0-25,000 cm^{-1}. As in our previous work [14], the absorption coefficients for H_2O and CO_2 at a spectral resolution of 0.005 cm^{-1} were computed from the BYU database generated from HITEMP 2010 for pressures from 0.1 to 50 and temperatures from 300 to 3000 K [21]. Soot particles are assumed to radiate in the Rayleigh regime [4] and the refractive index is obtained from Ref. [22].

2.1. Narrow-band Correlated-K distribution (NBCK) models

The NBCK model is used as benchmark to evaluate the simplified ω-ALDF based RCFSK model. Our previous studies demonstrated that the NBCK provides spectrally-integrated radiative outputs with maximum errors within 2% of line-by-line (LBL) solutions with a tiny fraction of the computational cost [23,24]. The NBCK solutions were performed with a spectral resolution of $\Delta\eta$ =25 cm^{-1}. The NBCK introduces on each narrow band (NB) a cumulative *k-g* distribution:

$$g^{NB}(k,\phi) = \frac{1}{\Delta\eta}\int_{\Delta\eta} H\left[k - \kappa_\eta(\phi)\right] d\eta \tag{1}$$

where κ_η is the spectral absorption coefficient, H is the Heaviside function, and $\phi = \{x_i, p, f_s, T\}$ is an array of state variables of the medium thermophysical properties, including the radiating species mole fraction, x_i, the pressure, p, the soot volume fraction, f_s, and the temperature, T. For the j^{th} band, centered at the wavenumber η_j, the NB radiative transfer equation (RTE) can be written as:

$$\frac{dI_{g_i}^j}{ds} = k_i^j(\phi)\left[I_{b\eta}(T) - I_{g_i}^j\right] \tag{2}$$

where g_i is a quadrature point of a 10- Gauss-Legendre quadrature ($N_G = 10$). The mean radiative intensity on the band, $\overline{I^j}$, and the total radiative intensity, I are given by:

$$\overline{I^j} = \sum_{i=1}^{N_G} I_{g_i}^j \omega_i \text{ and } I = \sum_{j=1}^{NB} \overline{I^j}\Delta\eta \tag{3}$$

where ω_i is the weight associated to g_i and NB the number of narrow band. On each NB, the absorption coefficient in Eq. (2) is obtained by solving:

$$g^{NB}(k_i, \phi) = g_i \tag{4}$$

In order to solve Eq. (4), separate databases of narrow band *k*-g distributions were constructed for CO_2 and H_2O from the LBL database described previously at the specific total pressures of interest for our simulations. The discretization in temperature was the same as for the LBL database and the following discretization in mole fraction was adopted: 0, 0.05, 0.1, 0.2, 0.3, 0.4, 0.6, 0.8, 1. For each narrow band, the NB *k-g* distributions were stored in the database for 128 points of a Gauss quadrature scheme [25]. The following procedure was used to determine k_i from Eq. (4) and the NB database. For each species, NB *k-g* distribution for each NB and each of the 128 Gauss points are interpolated from the database to provide single species *k-g* distribution in the thermophysical state ϕ. Linear interpolations and spline interpolations are performed on mole fraction and temperature, respectively [25]. For each NB, a mixed *k-g* distribution is then obtained at the 128 Gauss points by using the mixing scheme of Modest and Riazzi [25] and adding the soot absorption coefficient. The absorption coefficients k_i at g_i are then extracted from this mixed *k-g* distribution through linear interpolation.

2.2. Simplified ALDF rank-correlated full spectrum k-distribution model

2.2.1. Full spectrum k-distribution model

The Full-spectrum *k*-distribution (FSK) models introduce a Planck-weighted cumulative *k-g* distribution, defined as [4]:

$$g^{FS}\left(k, \underline{\phi}, T_p\right) = \int_0^{+\infty} H\left[k - \kappa_\eta\left(\underline{\phi}\right)\right] \frac{I_{b\eta}\left(T_p\right)}{I_b\left(T_p\right)} d\eta \tag{5}$$

where T_p, H and k are the Planck temperature, the Heaviside function, and a given value of the absorption coefficient. I_b is the Planck blackbody intensity. The full spectrum RTE is expressed as [4]:

$$\frac{dI_{g_i}}{ds} = k_i\left[a_i I_b(T) - I_{g_i}\right] \quad (6)$$

where g_i corresponds to a quadrature-point of a N_g-point Gauss-Legendre quadrature scheme (N_g =4, 8, 16, 32, etc.) and I_{g_i} is the radiative intensity at this quadrature point. In the present study, N_g was set to 16.

2.2.2. The RCFSK scheme

The concept of rank correlated spectrum was first developed for SLW methods [12] before being applied to the FSK methods [13]. Its main advantage is to avoid recourse to any reference state to make calculations in non-uniform media [12]-[14].

In this scheme, the absorption coefficient, $k(g_i)$, and the stretching function, $a(g_i)$, in Eq. (4) are obtained as follows:

$$g^{FS}\left(k_i, \underline{\phi}, T_p\right) = g_i \quad (7)$$

$$a_i = \frac{g^{FS}\left[k_i, \underline{\phi}, T\right] - g^{FS}\left[k_{i-1}, \underline{\phi}, T\right]}{g_i - g_{i-1}} \quad (8)$$

The total radiative intensity can then be computed as:

$$I = \sum_{i=1}^{N_G} I_{g_i} \Delta g_i \text{ with } \Delta g_i = g_i - g_{i-1} \quad (9)$$

This RCFSK method was found in our previous works to be only weakly sensitive to the choice of Planck blackbody temperature in conditions representative of combustion applications [14]. For reason that will be clarified in the next section, T_p was fixed to 1500 K in the present study.

For each pressure of interest, a full spectrum database was generated from the NB database described in Section 2.1 in order to determine g^{FS} which appears in Eqs. (7) and (8). Full

spectrum *k-g* distributions were generated for mixtures of CO_2, H_2O and soot for stored in the database for 32 values of *g* corresponding to a 32-point Gauss quadrature scheme and the same set of temperatures and mole fractions as in the NB database. The soot volume fraction space was discretized into 6 values between 0 and 10^{-5} (0, 0.5×10^{-6}, 1.0×10^{-6}, 1.5×10^{-6}, 2.0×10^{-6}, 1.0×10^{-5}). As discussed previously the Planck blackbody temperature was set to 1500 K. For each specific values of ϕ, FS k-g distributions were assembled from the following procedure [25]: i) NB *k-g* distributions are mixed, ii) the absorption coefficient of soot is added to the mixed NB cumulative *k*-distributions, and iii) finally, the mixture FS *k-g* distributions are assembled from the previously computed mixed NB *k-g* distributions. The required *k-g* distributions at a given computational point are obtained from the database by using linear interpolations on x_{CO2}, x_{H2O} and f_s and spline interpolations on T.

2.2.3. Planck temperature-based on the equiprobability of thermophysical states

The concept of ω-ALDF was introduced recently [16] in order to avoid the specification of a Planck blackbody source temperature for the construction of FS gas radiation models. ω-ALDFs are defined as:

$$g_{\omega}^{FS}(k,\phi) = \int_0^{+\infty} H\left[k - \kappa_{\eta}(\phi)\right] \omega(\eta) d\eta \tag{10}$$

where ω is the normalized spectral weighting function:

$$\omega(\eta) = \int_0^{+\infty} f(T) \frac{I_{b\eta}(T)}{I_b(T)} dT \tag{11}$$

In Eq. (11), f is the fraction of the volume occupied by the absorbing molecules evaluated over the computational domain where the gas temperature is lower than T. In Ref. [16], this

formalism was validated on several test cases using f functions defined on a case-by-case basis, using the data related to the various situations investigated. In the present work, our objective is to use the same idea of ω-ALDF but over a set of test cases for which no detailed information on the profiles of temperature and species concentrations is known in advance, as is the actual situation in CFD modelling of combustion processes. Consequently, the same approach as used in Ref. [16] cannot be applied directly but needs some adaptations. Without any other constraint than the limits that can be imposed by the source temperature, the most reasonable choice for f is the maximum entropy solution based on the only information on the support of the function. In other words, the most reasonable choice for f is, in this case, the uniform distribution over the minimum and maximum temperatures that one can expect to encounter over the set of tests cases, *i.e.*:

$$f(T) = \frac{1}{T_{max} - T_{min}} \tag{12}$$

It should be noticed here that the choice of a uniform f assumes that without any further information (details on the particular case treated) all thermophysical states have *á priori* the same probability. The interval $[T_{min}, T_{max}]$ was set in this work to the full range of available line by line data, viz. to the interval $[300K, 3000K]$. The corresponding weighting function ω is depicted in Figure 1a (plain bold red line), and is compared to the Planck spectral distribution at several temperatures.

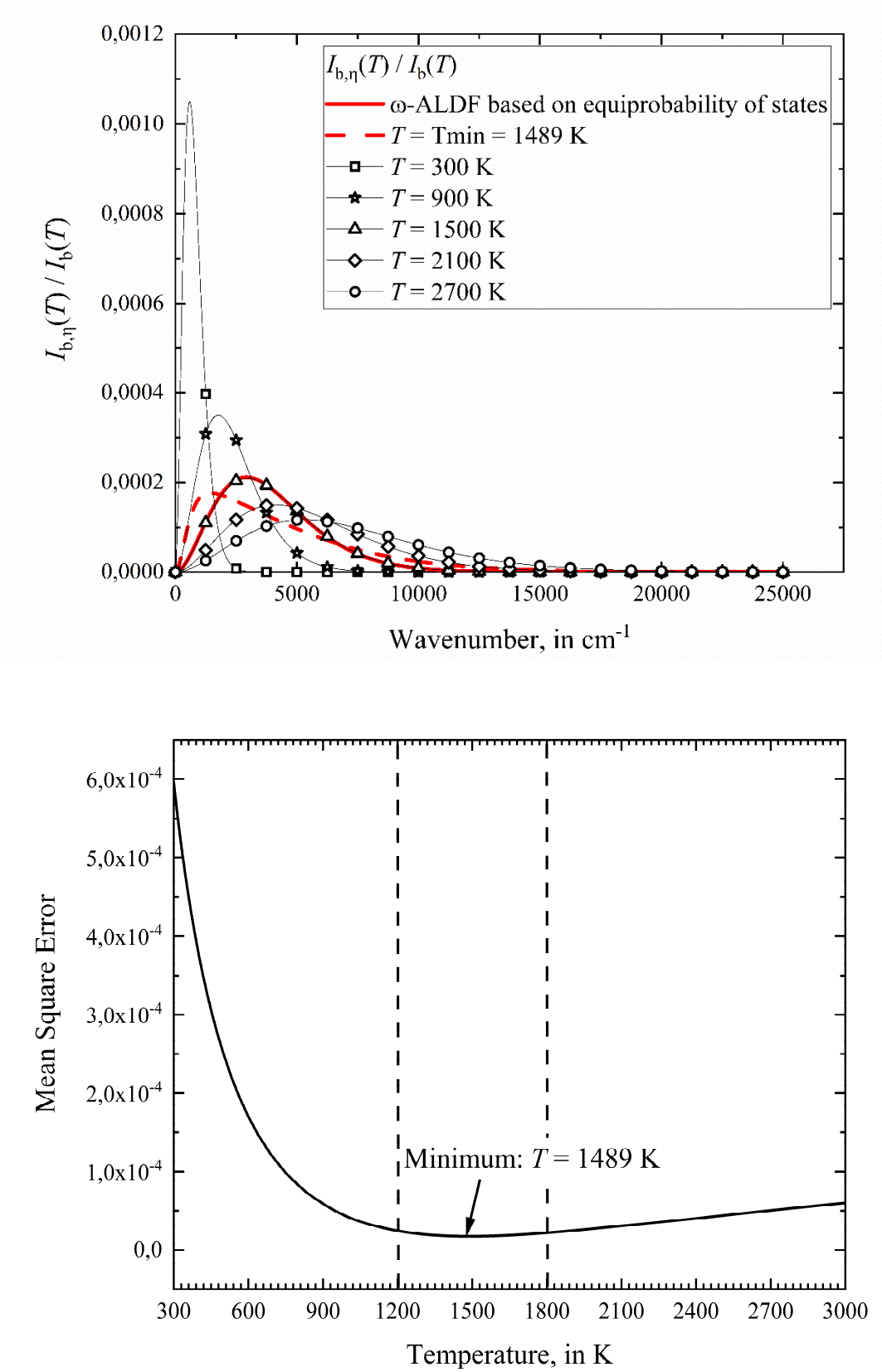

Figure 1. ω-ALDF and its approximation using an ALBDF. Top 1-a, bottom 1-b

The weighting function ω based on the assumed uniform f function can be used directly to generate a model database. However, in order to simplify the problem further and to make it applicable to possible users of the present method (for other ranges of intervals $[T_{min}, T_{max}]$ for instance), we propose here a method that allows approximating this ω-ALDF using a single, fixed Planck blackbody temperature. Our objective is thus to show that an approximation of the ω-ALDF function based on equiprobability of states is sufficient to make reliable radiative transfer calculations. For this purpose, we seek to determine a Planck blackbody temperature whose Planck spectral distribution provides the best approximation of the weighting function set $\omega$by Eqs. (12, 13) by an ALBDF. More formally, we define a temperature T_ω that minimizes the Mean Square Error (MSE):

$$MSE = \int_0^{+\infty} \left[\frac{I_{b\eta}(T_\omega)}{I_b(T_\omega)} - \omega(\eta) \right]^2 d\eta = \int_0^{+\infty} \left[\frac{I_{b\eta}(T_\omega)}{I_b(T_\omega)} - \int_{T_{min}}^{T_{max}} \frac{I_{b\eta}(T)}{I_b(T)} \frac{dT}{T_{max} - T_{min}} \right]^2 d\eta \quad (13)$$

This minimization process was solved graphically by plotting the MSE as a function of T_ω as shown in Figure 1b. The MSE exhibits a minimum error at a temperature T_ω = 1489 K, which is very close to the temperature obtained by trial and error and applied successfully in Refs. [17]-[20]. It is also noted in Fig. 1b that the minimum in MSE is quite broad, with the error nearly invariant in the range 1200-1800 K. As shown in Figure 1a (dotted bold red line), this selection of Planck blackbody temperature yields a reasonable approximation by an ALBDF of the true ωfunction based on a uniform f. Furthermore, as RCFSK/RCSLW models have been demonstrated to be rather insensitive to the choice of the Planck blackbody temperature, at least in the neighborhood of the optimum [14], the full model database was in practice constructed at the temperature of T_ω =1500 K ≈ 1489 K. One can notice that the temperature T_ω obtained through the theoretical justification of the ω-ALDF formalism differs significantly from the temperature that would be obtained by using the same assumption of equiprobability of states

together with a mean temperature. Indeed, this mean temperature approach would yield, with the same interval $[T_{min}, T_{max}]$, a Planck blackbody temperature of 1650 K. Using the average of the fourth-power of temperature provides 2059 K which is even higher than the mean temperature. Neither of these two temperatures produce an ALBDF that is remotely close to the ω-ALDF shown in Fig. 1a.

3. Test cases and metrics

3.1. Test cases

The assessment of the simplified ω-ALDF rank correlated full-spectrum k-distribution model is performed in decoupled radiative heat transfer calculations. The thermal fields, including gas temperature, mole fractions of CO_2 and H_2O, and soot volume fraction, required to run these calculations have been obtained from the simulations of axisymmetric turbulent jet non-premixed flames burning in air with the state-of-the-art Reynolds-Averaged Navier-Stokes (RANS)/flamelet/transported Probability Density Function (PDF) model described in detail in Refs. [26],[27]. These simulations were already published by the authors [28]-[31] and demonstrated to reproduce with fidelity the flame structures, including statistics of temperature, species concentrations, soot volume fractions, the subtle flow/chemistry/soot production radiation interactions, and the radiative characteristics of these flames, including radiant fractions and radiative heat fluxes. These simulations were performed with a wide band correlated k model.

The eight test flames, selected for the evaluation of the simplified ALDF RCFSK model, are summarized in Table 1 with the corresponding references. In this table, d, U_{inj}, P, H_f and, $f_{s,max}$ represent the fuel injection diameter, the fuel injection velocity, the pressure, the flame height, defined based on the isotherm 1500 K, and the peak of soot volume fraction. $\dot{Q}_{abs}/\dot{Q}_{em}$ and $\dot{Q}_{em,s}/\dot{Q}_{em}$ denote the ratio between total absorption, $\dot{Q}_{abs}$, and total emission, $\dot{Q}_{em}$, which characterizes the flame self-absorption and, in turn, the flame optical-thickness, and the ratio of

the total emission due to soot, $\dot{Q}_{em,s}$, to the total emission, which quantifies the contribution of soot.

The first flame corresponds to the lab-scale hydrogen flame investigated experimentally by Barlow and co-workers at SANDIA [32],[33]. The second flame has the same injection properties as the first but operates at a pressure of 30 atm and was specifically designed to illustrate the effects of pressure on gas radiation [28]. The third flame corresponds to the large-scale vertical hydrogen-jet flames, investigated experimentally by Schefer et al. [34]. In the experiments, hydrogen was released from high pressure storage tubes with a pressure decreasing exponentially from its initial value of 413 bar to near atmospheric pressure over a period of approximately 500 s. At these pressures, an under-expanded jet is observed with the flow being choked at the jet exit with an exit pressure considerably greater than the atmospheric one. The flame considered corresponds to conditions at $t = 10$s. The values in parentheses in Table 1 correspond to the effective injection conditions that reflect the conditions of the jet after expanding to the atmospheric pressure through a series of expansion shocks. These conditions were used in CFD simulations to simplify the injection problem [29]. The fourth and five flames are synthetic lab-scale methane flames at atmospheric pressure and at 4 atm, respectively. They were designed to investigate the effects of pressure on sooting flames [30]. Flame 6 is the lab-scale ethylene turbulent jet diffusion flame investigated experimentally by Lee et al. [35]. Flames 7 and 8 are synthetic flames that were generated by scaling the fuel injection diameter of flame 6 by factors 10 and 50, respectively, significantly increasing the flame height and the soot content [31]. Table 1 shows that the selected flames cover a wide range of sizes, optical thicknesses and sooting propensities. All the flames are dominated by gas radiation except flames 6 and 7, where soot and gas radiation have a similar contribution, and flame 8 where the soot contribution dominates.

Table 1. Turbulent jet diffusion flames used as test cases. The references indicate the article where the corresponding RANS/flamelet/Transported PDF simulation was reported.

N°	Fuel	d (mm)	U_{inj} (m/s)	P (atm)	H_f (m)	$\dot{Q}_{abs}/\dot{Q}_{em}$ (-)	$\dot{Q}_{em,s}/\dot{Q}_{em}$ (-)	$f_{s,max}$ (ppm)	Ref.
1	H_2	3.75	296	1	0.69	0.20	0	0	[28]
2	H_2	3.75	296	30	0.76	0.69	0	0	[28]
3	H_2	5.08 (51.5)	1259 (2047)	1	10.00	0.65	0	0	[29]
4	CH_4	2.50	130	1	0.68	0.36	0.013	0.031	[30]
5	CH_4	2.50	130	4	0.63	0.50	0.33	4.15	[30]
6	C_2H_4	2.18	48.7	1	0.50	0.25	0.49	2.06	[31]
7	C_2H_4	21.8	48.7	1	3.22	0.59	0.54	3.86	[31]
8	C_2H_4	109.0	48.7	1	13.2	0.84	0.68	10.8	[31]

3.2. Metrics

In our simulations, both narrow band and full spectrum RTE are solved with the axisymmetric formulation of the Finite Volume Method [36] with 12 × 16 control angles. Relative errors on the divergence of the radiative flux, $\boldsymbol{\nabla \cdot \dot{q}''_R}$, and on the vertical profile of incident heat flux at the radial boundary of the computational domain, $\dot{q}''_{R,w}$, will serve as metrics to evaluate the simplified ω-ALDF RCFSK model. The relative error for a given computed variable φ is defined as:

$$Error = |\varphi_{RCFSK} - \varphi_{NBCK}|/\max(|\varphi_{NBCK}|) \times 100 \text{ (in \%)} \quad (14)$$

4. Results and Discussion

Figures 2 and 3 show the comparison between the benchmark NBCK and the simplified ω-ALDF based RCFSK model for the flames 3 and 8, respectively. These flames were selected for illustration since they have the largest optical thicknesses among the non-sooting and sooting flames, respectively. Figure 2 shows that both fields of the radiative source term and heat flux at the boundary of the computational domain predicted by the simplified ω-ALDF

based RCFSK are almost indistinguishable from the reference solution for a large -scale H_2/air flame representative of hydrogen leakage hazard.

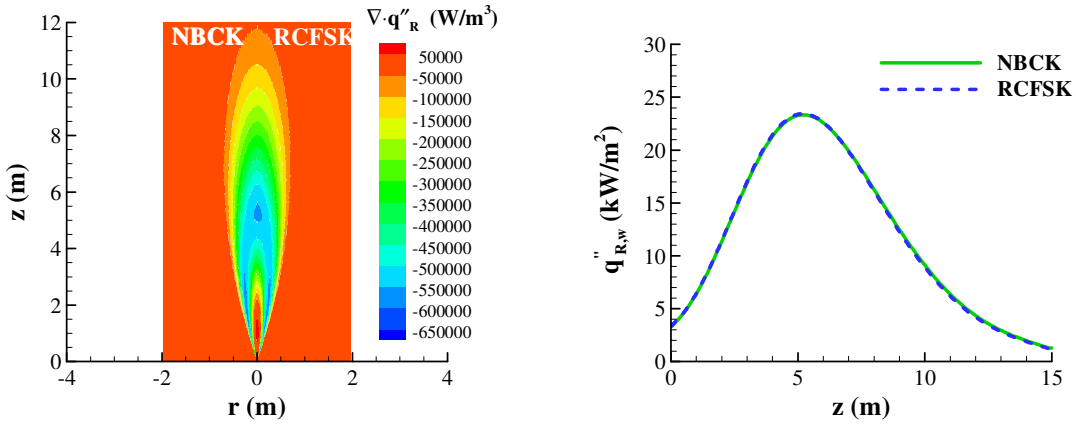

Figure 2. Comparison between NBCK and RCFSK predictions for flame 3. Left diagram: radiative source term (W/m^3), right diagram: flux at the boundary of the computational domain.

Figure 3 shows that, although a slight underprediction of the radiative flux is observed at the flame peak, a similar accuracy is obtained for a large-scale C_2H_4/air flame in which 84% of emission is reabsorbed within the flame. The field of the radiative source term indicates that the core of the flame is dominated by absorption (positive values of the radiative source term) whereas the wings and the upper part are dominated by emission. The capability of the RCFSK to capture radiative heat transfer in both region is clearly demonstrated.

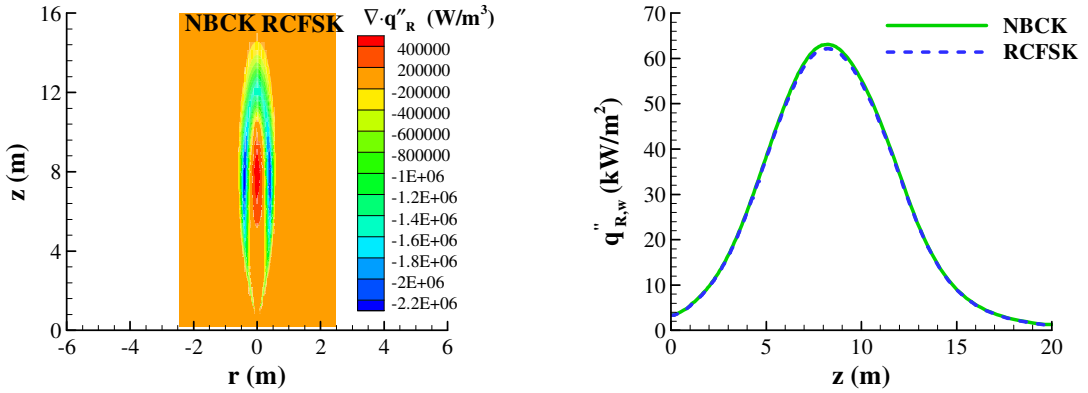

Figure 3. Comparison between NBCK and RCFSK predictions for flame 8. Left diagram: radiative source term (W/m^3), right diagram: flux at the boundary of the computational domain.

A quantitative comparison is summarized in Table 2 that details the mean and maximum relative errors for the eight test cases of Table 1. These results confirm that the simplified ω-ALDF based RCFSK method provides local spectrally-integrated radiative outputs in very close agreement with the NBCK method for a wide range optical thickness and soot radiation contributions. The largest errors of about 3-4% are observed for flames 1 to 4 that are characterized by either the absence of soot or low soot radiation (see the 8th column of Table 1). These results suggest that the simplified ω-ALDF RCFSK model yields very good predictive accuracy over a wide range of combustion conditions. It should be point out that decoupled radiative calculations provide the upper bound for the deviation between the model and the reference solutions. These discrepancies are expected lower in coupled simulations.

Table 2: Maximum and mean relative errors on the divergence of the radiative flux and on the wall heat flux.

Flame N°	Relative error on $\dot{q}''_{R,w}$ (%)		Relative error on $\nabla \cdot \dot{q}'_R$ (%)	
	Max	Mean	Max	Mean
1	2.70	1.80	3.87	0.63
2	1.29	0.66	1.18	1.08
3	0.90	0.46	3.17	0.16
4	3.03	1.96	2.19	0.57
5	2.28	1.01	1.48	0.84
6	0.75	0.50	0.64	0.08
7	0.75	0.31	1.03	0.88
8	1.46	0.63	1.33	0.13

Fixing the Planck blackbody temperature to a constant value T_ω has three significant advantages for CFD applications of turbulent flames:

1) It avoids possible sources of uncertainties related to the definition of an arbitrary Planck blackbody source temperature, especially in the case of turbulent flames. This also leads to a gain in terms of CPU (Central Processing Unit) cost as no "reference" Planck temperature needs to be defined on a case-by-case basis.
2) It simplifies the application and improves the computational efficiency of the method since the size of the look-up table for the RCSFK parameters k and a is reduced by one dimension, dramatically reducing the size of the database needed and the associated interpolation cost. Indeed, there is no need to generate a look-up table that involves the source temperature as input. Table 3 illustrates the CPU times related to the interpolation process and RTE integration for both the RCFSK and the simplified ω-ALDF RCFSK in the case of flame 8 over spatial and angular meshes with 4482 cells and 12×6 control angles, respectively. For these axisymmetric simulations, the interpolation process contributes for a significant part to the overall CPU time. Suppressing the Planck temperature from the database reduces the CPU time related to the interpolation procedure from 0.175 s to 0.112 s, this reduction being non-linear as a spline

interpolation is considered for temperatures whereas linear interpolations are applied for species and soot [25].

Table 3: CPU times in second for flame 8. The simulations were performed on a six core Intel i7-10850H (2.70GHz) processor computer.

	RCFSK	Simplified ω-ALDF RCFSK
Interpolation	0.175	0.112
RTE solver	0.125	0.125
Total	0.300	0.237

3) In addition, k and a then depend only on local scalars, namely x_{CO2}, x_{H2O}, f_S and T. Consequently, these quantities can be efficiently stored in a look-up table in conjunction with flamelet models as they are directly related to the reduced set of manifolds [17]-[20], [37].

5. Conclusions

This work presents a simplified version of the ω-absorption line distribution function for rank correlated full-spectrum k-distribution models. For this purpose, the ω-ALDF based on the assumption of equiprobability of states is approximated by an ALBDF based on a Planck blackbody temperature which was estimated theoretically to be about 1500 K (1489 K). The temperature is entirely defined by the specification of the ω-ALDF. The model was assessed by comparison with narrow band model calculations through the simulations of turbulent axi-symmetric non-premixed jet flames covering a wide range of optical-thicknesses and soot volume fractions. The predictions are within few percents of the reference solution. The main

interest in this approach lies on the improvement of the computational efficiency of the flame radiation model in view of high-fidelity combustion simulations.

References

[1] Modest MF, Haworth DC. Radiative Heat Transfer in Turbulent Combustion Systems: Theory and Applications. Springer, 2016. https://doi.org/10.1007/978-3-319-27291-7.

[2] Denison MK, Webb BW. The spectral line-based weighted-sum-of-gray-gases model in non-isothermal non-homogeneous media. ASME J. Heat Transf. 1995; 117: 359-365. https://doi.org/10.1115/1.2822530.

[3] Modest MF, Zhang H. The full-spectrum correlated-k distribution for thermal radiation from molecular gas-particulate mixtures. ASME J. Heat Transf. 2002; 124: 30-38. https://doi.org/10.1115/1.1418697.

[4] Modest MF, Mazumder S. Radiative Heat Transfer, 4th Ed. Academic Press, 2022.

[5] Liu F, Consalvi JL, Coelho PJ, André F, Gu M, Solovjov V, Webb BW. The impact of radiative heat transfer in combustion processes and its modeling – with a focus on turbulent flames. Fuel 2020; 281: 118555. https://doi.org/10.1016/j.fuel.2020.118555.

[6] Wang C, He B, Modest MF, Ren T. Efficient full-spectrum correlated-k-distribution look-up table, J. Quant. Spectrosc. Radiat. Transf. 2018; 219: 108-116. https://doi.org/10.1016/j.jqsrt.2018.04.002.

[7] Wang C, He F, Modest MF. Full-spectrum correlated-k-distribution look-up table for radiative transfer in nonhomogeneous participating media with gas-particle mixtures. Int. J. Heat Mass Transf. 2019; 137: 1053-63. https://doi.org/10.1016/j.ijheatmasstransfer.2019.03.149.

[8] Pearson JT, Webb BW, Solovjov VP, and Ma J. Efficient representation of the absorptionline blackbody distribution function for H2O, CO2, and CO at variable temperature, mole

fraction,and total pressure. J. Quant. Spectr. Rad Transfer 2014; 138: 82–96. https://doi.org/10.1016/j.jqsrt.2014.01.019.

[9] Zhou Y, Wang C, Ren T. A machine learning based efficient and compact full-spectrum correlated k-distribution model. J. Quant. Spectr. Rad Transfer 2020; 254: 107199. https://doi.org/10.1016/j.jqsrt.2020.107199.

[10] Zhou Y, Wang C, Ren T, Zhao C. A machine learning based full-spectrum correlated k-distribution model for nonhomogeneous gas-soot mixtures. J. Quant. Spectr. Rad. Transfer 2021; 268: 107628. https://doi.org/10.1016/j.jqsrt.2021.107628.

[11] Cai J, Modest MF. Improved full-spectrum k-distribution implementation for inhomogeneous media using a narrow-band database. J. Quant. Spectrosc. Radiat. Transfer 2014; 141: 65-72. https://doi.org/10.1016/j.jqsrt.2014.02.028.

[12] Solovjov VP, André F, Lemonnier D, Webb BW. The rank correlated SLW model of gas radiation in non-uniform media. J. Quant. Spectrosc. Radiat. Transfer 197; 2017: 26-44. https://doi.org/10.1016/j.jqsrt.2017.01.034.

[13] Solovjov VP, Webb BW, André F. The Rank Correlated FSK Model for Prediction of Gas Radiation in Non-Uniform Media, and its relationship to the Rank Correlated SLW Model. J. Quant. Spectrosc. Radiat. Transfer 2018; 214, 120-32. https://doi.org/10.1016/j.jqsrt.2018.04.026.

[14] Consalvi JL, André F, Coelho FR, Franca FHR, Nmira F, Galtier M, Solovjov V, Webb BW. Assessment of engineering gas radiative property models in high pressure turbulent jet diffusion flames, J. Quant. Spectrosc. Radiat. Transfer 2020; 253: 107169. https://doi.org/10.1016/j.jqsrt.2020.107169.

[15] Wang C, Modest MF, Ren T, Cai J, He B. Comparison and refinement of the various full-spectrum k-distribution and spectral line weighted-sum-of-gray-gases models for

nonhomogeneous media, J. Quant. Spectrosc. Radiat. Transfer 2021: 271; 107695. https://doi.org/10.1016/j.jqsrt.2021.107695.

[16] André F, Solovjov VP, Webb BW. The ω-absorption line distribution function for rank correlated SLW model prediction of radiative transfer in non-uniform gases, J. Quant. Spectrosc. Radiat. Transfer, vol. 280, pp. 108081, 2022. https://doi.org/10.1016/j.jqsrt.2022.108081

[17] Nmira F, Consalvi JL. Local contributions of resolved and subgrid turbulence-radiation interaction in LES/presumed FDF modelling of large-scale methanol pool fires. Int. J. Heat Mass Transfer 190; 2022: 122746. https://doi.org/10.1016/j.ijheatmasstransfer.2022.122746

[18] Nmira F, Ma L, Consalvi JL. Influence of gas radiative property models on Large Eddy Simulation of 1 m methanol pool fires. Combust. Flame 2020 ; 221 : 352-363. https://doi.org/10.1016/j.combustflame.2020.08.005.

[19] Nmira F, Ma L, Consalvi JL. Assessment of subfilter-scale turbulence radiation interaction in non-luminous pool fires. Proc. Combust. Inst. 2021; 38 : 4927-34. https://doi.org/10.1016/j.proci.2020.06.271

[20] Nmira F, Bouffard A, Consalvi JL, Wang Y. Large-eddy simulation of lab-scale ethylene buoyant diffusion flames: Effects of subgrid turbulence/soot production interaction and radiation models. Proc. Combust. Inst. 2023; 39: 3959-68. https://doi.org/10.1016/j.proci.2022.07.004.

[21] Pearson JT, Webb BW, Solovjov VP, Ma J. Updated correlation of the absorption line blackbody distribution function for H2O based on the HITEMP2010 database, J. Quant. Spectrosc. Radiat. Transfer 2013;128:10-17. https://doi.org/10.1016/j.jqsrt.2012.07.016.

[22] Chang H and Charalampopoulos T. Determination of the wavelength dependence of refractive indices of flame soot. Proc. R. Soc 1990; 430: 577-591. https://doi.org/10.1098/rspa.1990.0107.

[23] Consalvi JL, Liu F. Radiative heat transfer in the core of axisymmetric pool fires – I: Evaluation of approximate radiative property models. Int. J. of Thermal Sci. 214;84:104-117. https://doi.org/10.1016/j.ijthermalsci.2014.04.018.

[24] Chu H, Consalvi JL, Gu M, Liu F. Calculations of radiative heat transfer in an axisymmetric jet diffusion flame at elevated pressures using different gas radiation models. J. Quant. Spectrosc. Radiat. Transfer 2017;197:2-25. https://doi.org/10.1016/j.jqsrt.2017.02.008.

[25] Modest MF, Riazzi RJ. Assembly of full-spectrum k-distributions from a narrow-band database; effects of mixing gases, gases and nongray absorbing particles, and mixtures with nongray scatterers in nongray enclosures, J. Quant. Spectrosc. Radiat. Transfer 2005; 90: 169-189. https://doi.org/10.1016/j.jqsrt.2004.03.007.

[26] Consalvi JL, Nmira F, Burot D. Simulations of sooting turbulent jet flames using a hybrid flamelet/stochastic Eulerian field method. Combust. Theor. Model. 2016; 20: 221-257. https://doi.org/10.1080/13647830.2015.1125024

[27] Consalvi JL, Nmira F. Transported scalar PDF modeling of oxygen-enriched turbulent jet diffusion flames: Soot production and radiative heat transfer. Fuel 2016; 178: 37-48. https://doi.org/10.1016/j.fuel.2016.03.035.

[28] Nmira F, Consalvi JL. Pressure effects on radiative heat transfer in hydrogen/air turbulent diffusion flames. J. Quant. Spectrosc. Radiat. Transfer 2018; 220: 172-179. https://doi.org/10.1016/j.jqsrt.2018.09.013.

[29] Consalvi JL, Nmira F. Modeling large-scale under-expanded hydrogen jet fires, Proc. Combust. Inst. 2019; 37: 3943-3950. https://doi.org/10.1016/j.proci.2018.05.022

[30] Nmira F, Liu Y, Consalvi JL, André F, Liu F. Pressure effects on radiative heat transfer in sooting turbulent diffusion flames, J. Quant. Spectrosc. Radiat. Transfer 2020 ; 24 : 106906. https://doi.org/10.1016/j.jqsrt.2020.106906

[31] Consalvi JL, Nmira F. Absorption Turbulence-Radiation Interactions in Sooting Turbulent Jet Flames, J. Quant. Spectrosc. Radiat. Transfer 2017; 201: 1-9. https://doi.org/10.1016/j.jqsrt.2017.06.024

[32] Barlow RS, Carter C.D. Raman/Rayleigh/LIF measurements of Nitric Oxide formation in turbulent hydrogen jet flames, Combust. Flame 1994; 97: 261-280. https://doi.org/10.1016/0010-2180(94)90020-5

[33] Frank JH, Barlow RS, Lundquist C. Radiation and nitric oxide formation in turbulent non-premixed jet flames. Proc. Combust. Inst. 2000; 28: 447-454. https://doi.org/10.1016/S0082-0784(00)80242-8

[34] Schefer RW, Houf WG, Williams TC, Bourne B, Colton J. Characterization of high-pressure, underexpanded hydrogen-jet flames, Int. J. Hydrogen Energy 2007; 31: 2081-2093. https://doi.org/10.1016/j.ijhydene.2006.08.037

[35] Lee SY, Turns SR, Santoro RJ. Measurements of soot, OH, and PAH concentrations in turbulent ethylene/air jet flames, Combust. Flame 2009; 156: 2264-2275. https://doi.org/10.1016/j.combustflame.2009.09.005

[36] Chui EH, Raithby GD, P. M. J. Hughes PMJ. Prediction of radiative transfer in cylindrical enclosures with the finite volume method, J. Thermophys. Heat Transfer 1992; 6: 605-611. https://doi.org/10.2514/3.11540

[37] Nmira F, Bouffard A, Consalvi JL. Flamelet/transported PDF simulations of ethylene/air jet turbulent non-premixed flame using a three-equation PAH-based soot production model. Combust. Theor. Model. 2023, https://doi.org/10.1080/13647830.2023.2224755